Flow Distribution Property of the Constructal Distributor and Heat Transfer Intensification in a Mini Heat Exchanger

Yilin Fan, Raphaël Boichot, Thierry Goldin, and Lingai Luo
Laboratoire Optimisation de la Conception et Ingénierie de l'Environnement (LOCIE), Université de Savoie, Campus Scientifique, Savoie Technolac, 73376, Le Bourget-Du-Lac Cedex, France

DOI 10.1002/aic.11597
Published online September 22, 2008 in Wiley InterScience (www.interscience.wiley.com).

This article reports a numerical and experimental study on flow maldistribution and heat transfer intensification in a mini heat exchanger with constructal distributor/collector integrated. The flow distribution characteristics of the constructal component functioning as a fluid distributor or as a fluid collector have been investigated and compared using computational fluid dynamics simulations. An experimental setup is designed and constructed for thermal and hydraulic performances tests. The effects of various assembly configurations on heat transfer characteristics and pressure drops are discussed. The results indicate that the integration of one constructal collector at the outlet of the heat exchanger can achieve almost uniform flow distribution and consequently better intensify the heat transfer. It is also the most advantageous configuration based on a balanced consideration of heat transfer intensification and pump power consumption under the investigation conditions. © 2008 American Institute of Chemical Engineers *AIChE J*, 54: 2796–2808, 2008

Keywords: heat transfer intensification, flow maldistribution, constructal component, distributor, collector, pump power consumption

Introduction

The deterioration in heat transfer of a multi-channel heat exchanger due to the flow rate (velocity) difference over the different channels, or "*Maldistribution*," is an important issue, especially, when the channels of the heat exchanger are in the range of micro- or mini-scale. Considerable attention has been paid to find effective solutions and thus intensify the heat transfer.

Besides the passage-to-passage flow maldistribution induced by manufacturing imperfections, fouling, condensable impurities, etc., the gross flow maldistribution which is generally associated with the improper entrance configuration of a fluid distributor (or the exit configuration of a fluid collector as well) has been well recognized.[1–14] Currently available research articles on this topic reveal that solutions can be mainly classified into two categories: the insertion of porous media and the modification of the distributor's geometrical parameters. More details are tabulated in Table 1. These two kinds of methods would both increase the pressure drop of the heat exchanger system as a compensation for more uniform flow distribution.

Novel fluid distributors were proposed by Tondeur and Luo[25,26] to equalize the flow distribution with the least increase of pressure drop. Their multi-scale internal channel structures are optimized by minimizing the viscous dissipation and the residence time simultaneously according to the "constructal theory."[27–29] Polymer prototypes of the constructal components were manufactured using Stereolithography[30,31] at the "Département de Chimie Physique des Réactions" in Nancy, France. These fluid distributors, along with other multi-scale components such as mixers, heat exchangers,[32] are to our knowledge the first series of "constructal" prototypes realized for engineering applications. After that, polymer constructal distributor prototypes were assembled with a mini crossflow heat-exchanger to

Correspondence concerning this article should be addressed to L. Luo at lingai.luo@univ-savoie.fr.

Table 1. Comparison on Solutions for Flow Maldistribution in Heat Exchangers

Reference	Study Type	Heat Exchanger Specification	Test Condition	Possible Solution	Conclusion
Lalot et al.[6]	E/N*	Graphite electrical heater; 128 channels; channel diameter: 9.52 mm;	Air; 10,000 < channel Re < 40,000	Uniformly perforated grid	Max/min velocity ratio drops from 4 to less than 1.5.
Jiao et al.[9]	E	Plate-fin heat exchanger; 1100 cold-flow passages ($9.5 \times 2 \times 0.3$ mm^3 fin demension); 1000 hot-flow passages ($6.5 \times 2 \times 0.3$ mm^3 fin demension)	Water; 1100 < Re inlet < 3000	Two stage distributing structure	Max/min velocity ratio drops from 2.1–2.8 to 1.2–1.4
Zhang and Li[15]	N	As above	500 < Re inlet < 3000	Two stage distributing structure	Flow nonuniformity reduced from 3.47 to 0.71
Jiao and Baek[12]	E	As above	Water; 1100 < Re inlet < 3000	Distributor's configuration parameter h/H	Max/min velocity ratio drops from 2.57–3.66 to 2.08–2.81
Wen et al.[16]	E	As above	Air; Re inlet: 6.0×10^4	Punched baffle	Max/min velocity ratio drops from 23.2 to 1.8; Heat exchanger effectiveness enhanced about 12%
Wen and Li[11]	N	Plate-fin heat exchanger; 43 micro passages	Re inlet = 100,000	Punched baffle	Max/min velocity ratio drops from 3.44–3.04 to 1.57–1.68
Kulkarni et al.[10]	N	Crossflow microchannel evaporator	Gas	Novel radial header instead of conventional longitudinal header	Flow maldistribution minimized
Tereda et al.[17]	E	U type plate heat exchanger; 26 plates, stainless steel, corrugated surface.	Water; 500 < Channel Re < 4000	–	Maldistribution increase with flow rate and decreases with port diameter
Bobbili et al.[8]	E	U type plate heat exchanger; 21 and 81 plates; stainless steel, low corrugation angel; 4.8 mm equivalent channel diameter	Water; 1000 < Channel Re < 17,000	Geometry of the connector and the channel port	Maldistribution increase with overall pressure drop
Galeazzo et al.[18]	E/N	Plate heat exchanger; four FT-43 12×8 cm^2 stainless steel flat plates; 3.0 mm equivalent diameter	Water; 100 < Re channel < 1500	–	CFD model takes into flow maldistribution
Wang and Wang[19]	E/N	Plate-fin catalytic combustion heat exchanger; Stainless steel 304	Gas; gas hourly space velocity between 2300 and 12,000 h^{-1}	T or Y type branched multi-scale distributor	Maldistribution factor drops from 7.14–11.74 to 4.92–6.9
Jones et al.[20]	E/N	Silicon microchannel heat sink; seventy-six 110 μm wide $\times$ 371 μm deep channels	Air; channel Re = 10.2 and 102	A rectangular manifold shape instead of the original streamline shape	Max/min velocity ratio drops from 1.34 to 1.05; 32.7% augmentation of total pressure drop
Luo et al.[21,22]	E/N	Mini crossflow aluminum heat exchanger; 128 channels for one fluid; channel diameter: 2.5 mm; channel length: 56.5 mm	Water; 50 < Channel Re < 250	Constrctal distributor/collector	Up to 30% augmentation of overall heat transfer coefficient; small increase of pressure drops
Habib et al.[23]	N	Air cooled heat exchanger; 32 tubes of diameter 25.65 mm	Hydrocarbon oil; Inlet flow velocity between 1 and 2.5 m s^{-1}	Geometry of the nozzles; two stage distributing structure	62.5% decrease in the standard deviation of the mass flow
Kim et al.[24]	N	Multi-pass, multi-channel aluminum heat exchanger block with outside fins; channel diameter: 10 mm; channel length: 420 mm	Air; Fully developed turbulent	Number of passes; inlet diameter	Flow maldistribution alleviated

*E, experimental; N, numerical.

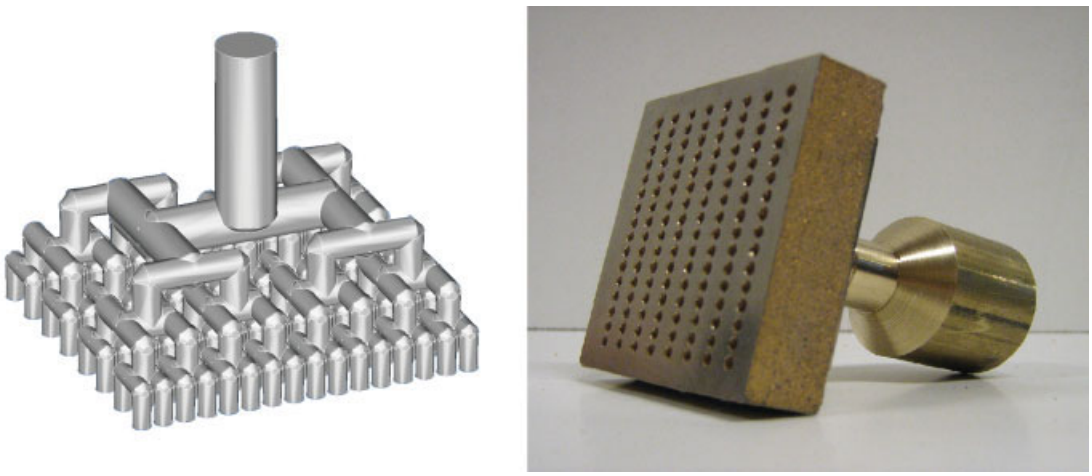

Figure 1. Prototype of the metallic multi-scale flow distributor and its inner channel structure.

[Color figure can be viewed in the online issue, which is available at www.interscience.wiley.com.]

evaluate the effects of flow distribution on its thermal and hydraulic performances by experiments[22] and by Computational Fluid Dynamics (CFD) simulations.[21] The preliminary results indicate that the integration of constructal distributor/collector can, to some extent, equalize the flow distribution and consequently enhance the heat transfer under laminar flow condition. The integration of one constructal collector at the outlet surface of the heat exchanger shows a better thermal performance. The encouraging conclusion is, however, limited in very small Re range ($50 <$ Channel Re < 250) with small temperature differences (0–30°C) of working fluids because of the physical property restrictions of polymer material: polymer prototypes are very fragile and cannot bear high temperature or high static and dynamic pressures.

The present study aims at extending the previous conclusion to a wide range of flow rate (average channel Re between 800 and 3500) and fluid temperatures (25–75°C) on one hand, and giving a comprehensive investigation of the flow distribution, thermal and hydraulic performances of a metallic constructal distributor/collector-mini heat exchanger system on the other hand. Both CFD simulation and experimental methods are employed. The enhancement of heat transfer realized by flow uniform distribution and the thermal-hydraulic balance are discussed. The results may provide some original information and thoughts to the design and optimization of heat exchangers and flow distribution/collection systems.

Devices

Mini crossflow heat exchanger

The mini heat exchanger used in this study is a single pass, both fluids unmixed crossflow heat exchanger manufactured in the "Laboratoire des Sciences du Génie Chimique" in Nancy, France. Two perpendicular sets of channels that are devoted to hot and cold fluids, respectively, were drilled in a cubic solid block of aluminum. Each set of channels is composed of 16 rows and 8 columns, the total number of channels thus being 128, all with the diameter of 2.5 mm and the length of 56.5 mm. Detail dimension parameters of the heat exchanger are given in Ref. 21.

Constructal component

The metallic constructal distributors were manufactured by CYBERSCULPTURE & CO SARL (Dombasle-en-Argonne, France), using direct metal powder stereolithography. The material used consists of 60% stainless steel and 40% bronze powder mixture (Norm S4). It has a good temperature and pressure proof nature allowing tests involving a wide range of temperatures and flow rates. Figure 1 shows a schematic view of the binary 3-D constructal component and its detail dimension parameters are given in Ref. 22. Conventional pyramidal distributors fabricated with the same metal material are introduced for comparison. Instead of the bifurcated interior structure, they show a simple pyramidal space from one inlet tube to a square surface.

Coupling multi-scale distributors with the heat exchanger

Previous study indicates that the levels of distribution uniformity reached may be different when the constructal component is used as a fluid distributor or as a fluid collector. To estimate the effect of flow distribution that is associated with the sort of inlet distributor or outlet collector or both, four configurations are considered as follows. Figure 2 gives an example of the test section (CEP) that is formed by the distributor, the heat exchanger, and the collector.

CEP: Constructal inlet – Exchanger – Pyramidal outlet;
PEC: Pyramidal inlet – Exchanger – Constructal outlet;
CEC: Constructal inlet – Exchanger – Constructal outlet;
PEP: Pyramidal inlet – Exchanger – Pyramidal outlet.

Flow Distribution

The application of exact visualization techniques such as the particle image velocimetry in this case is difficult, not only because of the relative small channel diameter but also

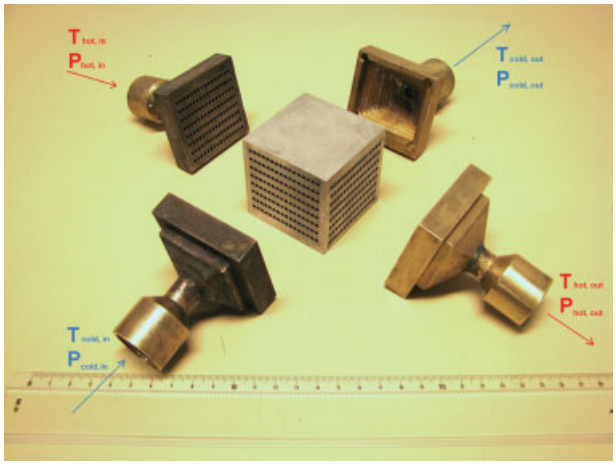

Figure 2. Photo of the test section configuration example (CEP).

[Color figure can be viewed in the online issue, which is available at www.interscience.wiley.com.]

because of the complexity of the 3-D geometry: channels hide themselves and couch together. As a result, CFD simulation tools are adopted here to obtain some general comprehensions of flow patterns in the channel structure of the constructal component.

The previous studies[21,22] found that the heat exchanger had better thermal performance and relative low pressure drops, whereas its outlet surface was equipped with a constructal collector (PEC). Now we try to explain this phenomenon explicitly from the flow distribution point of view. That is, *the flow distribution in the PEC is more uniform than that in the CEP and, in consequence, leading to a better thermal performance of the exchanger*. This section deals with comparative simulations realized with the aim of investigating the influence of fluid direction on the flow patterns and the flow maldistribution in the constructal component. The simulations take into account the multi-scale channels in the constructal component and the parallel channels of the heat exchanger as well.

Numerical simulation

The software GAMBIT was used to build up and mesh the geometry model of the constructal component. Smooth transition was introduced at the junctions and channel turns. Unstructured tetrahedral regular elements were applied for meshing the computational project. A meshing validity study was made to be sure that it does not influence the results. Note that with the symmetric assumption, one quarter of the real object was adopted as the model for the purposes of lessening the computational burden.

Pure water was used as working fluid with the assumptions of steady-state incompressible hydrodynamics and isothermal conditions. The boundary conditions were the same for the distributor case and the collector case. At the inlet port, a constant velocity normal to the entry surface was used as initial boundary condition. All of the 32 outlet ports were defined as pressure-outlet, with a zero relative pressure. Walls were set with a no-slip condition. Finally, two axes of symmetry were set.

The FLUENT software package was employed as the equation solver to solve Navier-Stokes equations. Turbulent segregated solver (RNG k-ε) was adopted, mainly because strong mixing and turbulence of fluid occur at elbows and bifurcations even under laminar flow conditions. The SIMPLE algorithm was selected to couple the velocity and the pressure, and the calculations were performed in double precision. The solution was considered to be converged when the sums of the normalized residuals for each control equations were all within the order of magnitude of 1×10^{-6}.

The relative flow rate deviation defined as the deviation of local flow rate at one port to the average value of flow rate is calculated and studied.

$$D_i = \frac{f_i - f_{\text{ave}}}{f_{\text{ave}}} \tag{1}$$

D_i: relative deviation of local flow rate at port i
f_i: value of flow rate at port i
f_{ave}: value of average flow rate

Another global parameter, namely, the maldistribution factor D_g is also employed for comparison.

$$D_g = \sqrt{\frac{1}{N-1}\sum_{i=1}^{N}\left(\frac{f_i}{f_{\text{ave}}} - 1\right)^2} \tag{2}$$

Here, N stands for the sampling outlets' number and it is 32. The smaller the values are, the more uniform the flow distribution is.

Influence of flow direction

In the view point of fluid dynamics, the behaviors of the flowing fluid inside the constructal component are rather complex because it may be far from fully developed flow conditions due to the strong influence of inner structure boundaries. Pressure drops or energy dissipations are generally produced by the sudden changes of flowing directions in the constructal component (bifurcations and 90° elbows). Figure 3 shows a comparison of velocity vectors passing through the channels of three horizontal layers with opposite directions. The total inlet velocity is 1 ms^{-1}, corresponding to an average Re of 127 in the smallest channels.

In the distributor case (left column of Figure 3), fluids with high velocity are generally located next to the wall of the channels. There is a strong viscous friction between the fluids and the wall. Moreover, fluids crush against the wall located in front of the flowing direction in the first horizontal layer, leading to the generation of vortex and turbulences and an immediate segregation of velocity vectors. Consequently, the flow rate in the "child" branch situated in the natural direction of the "mother" channel increases. It can also be observed that vortex and turbulences are still in presence in the channels of the second and third layers. As a result, flow rates at outlet channels are not equal; flow maldistribution still exists. Note that even under the theoretical laminar flow condition, which meets the average Reynolds criteria (Re channel = 127), the flow patterns are locally turbulent as the values of local Re could be very high. In gen-

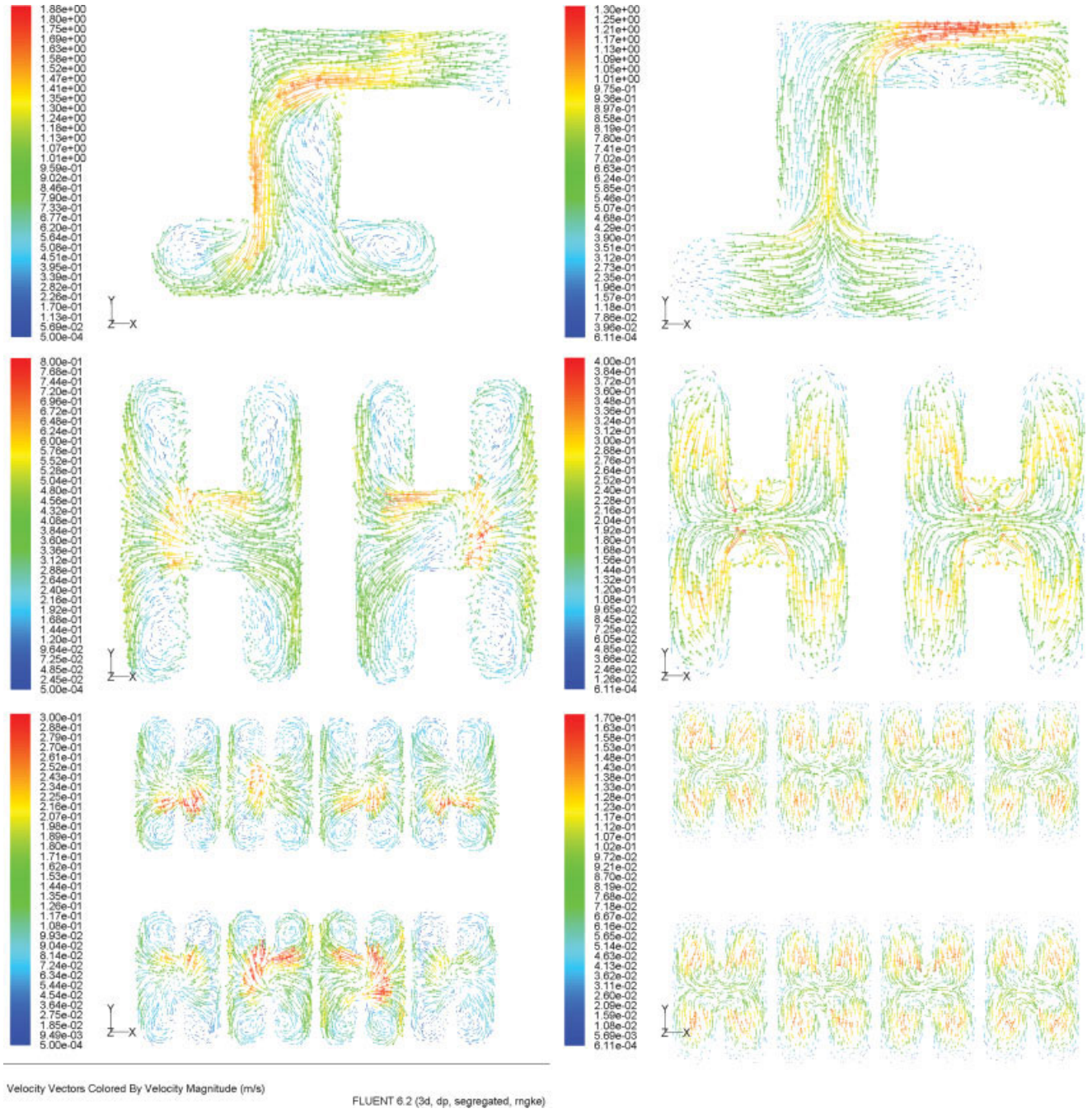

Figure 3. Velocity vectors in the channels of three horizontal distribution layers of the constructal component (left: distributor; right: collector).

[Color figure can be viewed in the online issue, which is available at www.interscience.wiley.com.]

eral, any change of flow velocity, in either direction or magnitude, can generate vortices that develop when normal streamlines are disturbed and when boundary layer separation occurs, as indicated in Figure 3.

On the other hand, in the collector case (right column of Figure 3), fluids with high velocity are generally situated at the center of the channels instead of against the walls. The velocity profile in each channel and the streamlines are well kept at each collecting level. Fluids are "aspired" from each inlet channel and mixed regularly at each converge point with less vortex or turbulences produced. The multi-scale structure of the constructal component works as a well-functioned fluid drainage device with the capability of approaching a uniform and stable flow distribution.

Figure 4 gives a comparison of the velocity magnitude in the smallest channels of the two cases. It is clear that in the collector case, the velocities in the inlet channels are almost identical, indicating perfect flow distribution (D_g = 0.23%). On the contrary, in the distributor case, the velocities in the outlet channels are not uniform (D_g = 17.02%). In conclu-

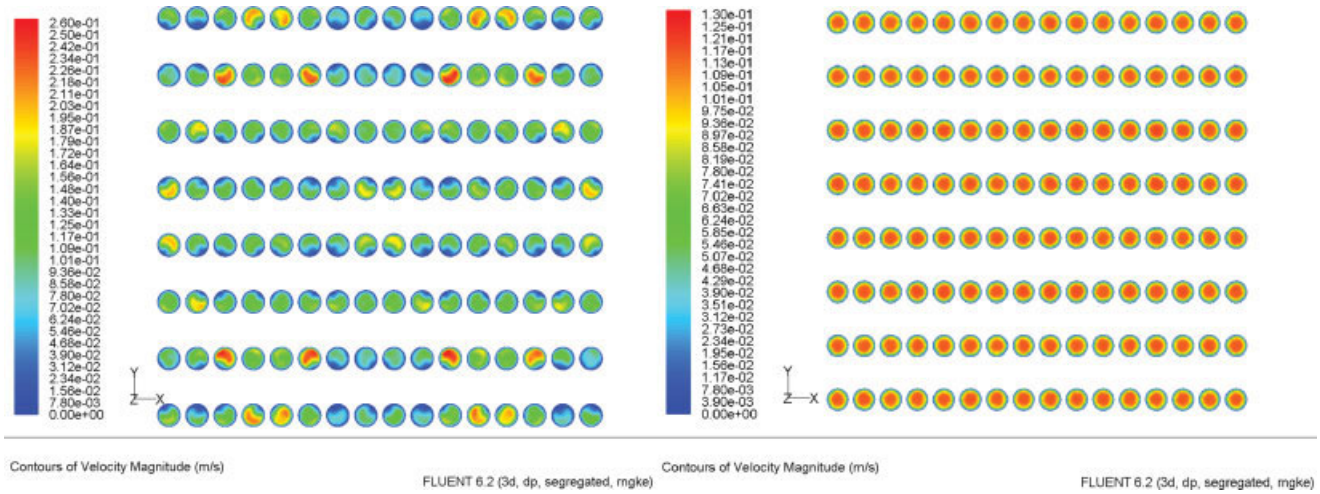

Figure 4. Contour of velocity magnitude in the smallest channels (left: distributor; right: collector).

[Color figure can be viewed in the online issue, which is available at www.interscience.wiley.com.]

sion, the constructal component used as a fluid collector, compared with the distributor case, can guarantee the more uniform flow distribution.

Robustness in relation to flow rate

The results of the relative flow rate deviation D_i with the total velocity (velocity in the single largest channel) ranging from 0.1 ms^{-1} to 10 ms^{-1} are reported in Figure 5. Table 2 also gives the simulated maldistribution factors D_g for several total velocities of fluids.

In the distributor case, the flow maldistribution becomes much more serious with the increasing of flow rate, because the inertial effect plays a dominant role under high flow rate condition. The D_g for the distributor case is in the order of magnitude of several tenth percent (about 40% maximum). On the contrary, the constructal component used as a fluid collector can always guarantee an almost uniform flow distribution, even under high flow rate conditions: the maximum D_g for the collector case is less than 3%, significantly lower than that in the distributor case.

It can be concluded with this comparison that the fluid direction in the constructal component has a great influence on the flow maldistribution. The constructal component integrated at the outlet surface of the heat exchanger seems to be more advantageous because of its uniform flow distribution capability and the robustness of this capability even under high total velocity conditions.

The significant difference in flow patterns implies that the flow direction may also have effects on the thermal and hydraulic performances of the heat exchanger system. Experimental results will be reported and discussed in the next section.

Experimental validation

A simple experiment of optical tracer visualization is conducted to validate the obtained numerical results, using a transparent polymer prototype. The idea here is to visualize the progression and the development of a small volume of black ink as tracer in interior channels and around the outlet surface of the prototype. Tests were repeated to verify that the progression process was reproducible.

Figure 6 gives a comparison of the simulation result and the picture recorded by a high-speed camera (PHOTRON PCI R2, 1000 images per second) of the outlet flow distribution. It can be observed that the two pictures share similar flow distribution behavior: there exits a residence time difference over different channels and some outlet ports are better supplied than the others. Undersupplied zones can be highlighted, mainly situated at the four corners and near the center of the upper and lower edges. Zones with oversupplied flows can also be located, mainly with a rhombus shape that intercepts the external outlet surface. Good agreement is found between simulation and experimental results.

The fluid flow is equally separated at the first and second splitting points because the four parts of the external surface (upper left, upper right, lower left, lower right) have almost the same distribution behavior. The final distribution is axisymmetric. The crash and bump between the fluid flow and the wall in front of the flowing direction generate vortex and turbulence and fluid with high velocity is located next to the channel wall, as shown in the distributor case in Figure 3. As a result, the "child" channel situated in the natural flow direction of the "mother" channel receives more fluid than the one in the opposite does. This is the initial predisposing cause of the final flow maldistribution. After that, the fluid flow is unequally separated at every splitting point, leading to the final shape shown in Figure 6. In the collector case, however, vortex and turbulence can generally be avoided and streamlines can be kept. The two "child" channels are expected to supply equal fluids to the mother channel, which mix regularly at every merge point, leading to the uniform flow distribution.

In Figure 6, the flow velocity at the single inlet channel (diameter = 8 mm) of distributor is 1.12 m s^{-1}, corresponding to the total flow rate of 2.2 liter per min and the Re of 900. The calculated average Re in the outlet channels (diameter = 2.5 mm) is 173. The observed flow turbulences con-

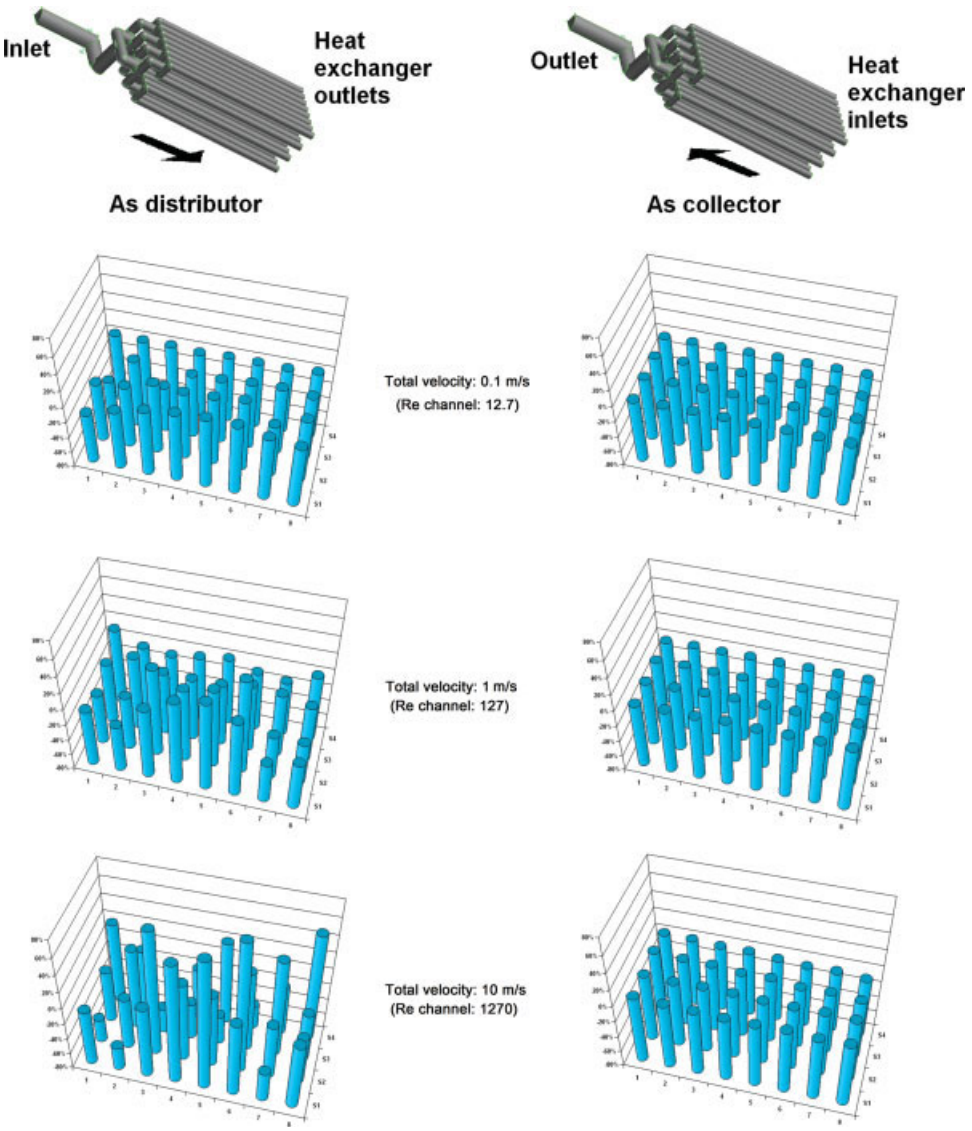

Figure 5. Comparison of D_i for constructal component used as distributor or as collector.

(Total velocity corresponds to the velocity in the largest channel; Re channel corresponds to the average Re number in the smallest channels). [Color figure can be viewed in the online issue, which is available at www.interscience.wiley.com.]

firm that the use of RNG k-ε model in the CFD simulation is suitable. Note that the flow distribution on the outlet surface of the distributor is generally symmetric, implying the validation of the representative quarter model set-up. Our next step is to verify the flow behavior in both distributor and collector cases using more advanced visualization techniques. And also, geometric modifications and optimizations are expected to alleviate the unequal flow distribution in the distributor case.

Thermal and Hydraulic Study

Now let us turn back to the notion of heat transfer intensification and the relationship between flow distribution and

Table 2. Comparison of the Maldistribution Factor D_g. and D_i

Velocity in the Largest Channel (m s^{-1})	Average Re in the Smallest Channels	D_g		$\|D_i\|$ Max	
		Distributor Case	Collector Case	Distributor Case	Collector Case
0.1	12.7	9.01%	0.51%	29.7%	0.5%
1	127	17.02%	0.23%	37.8%	1.3%
10	1270	40.15%	2.85%	85.4%	6.4%

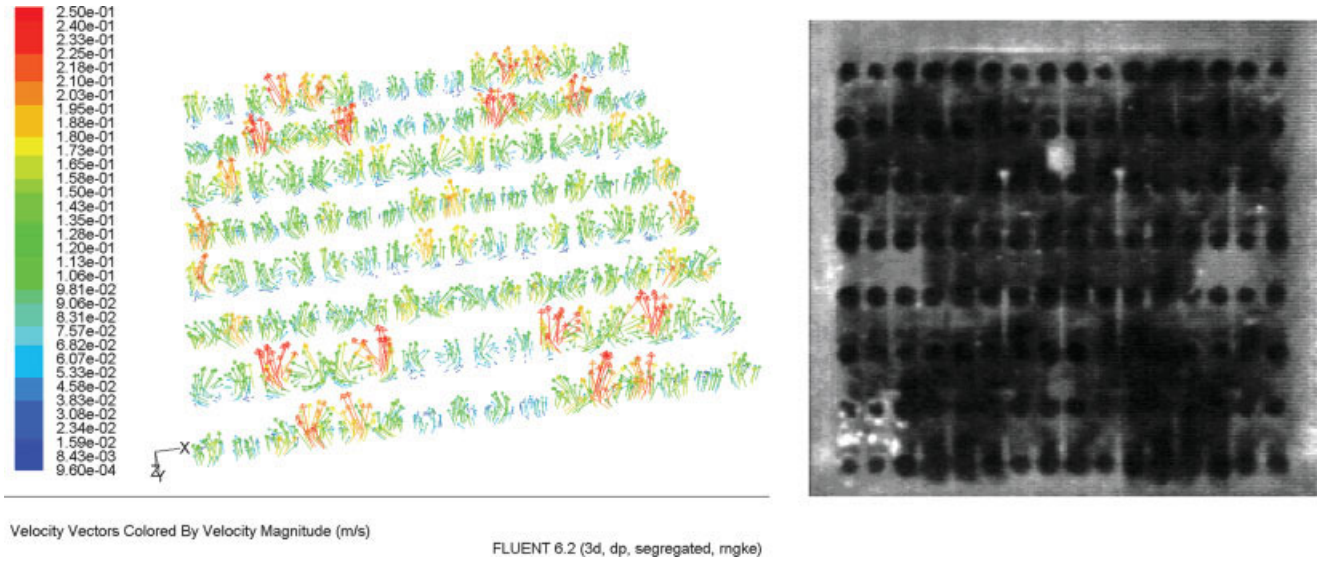

Figure 6. Comparison of simulation and experimental results of outlet flow distribution.

[Color figure can be viewed in the online issue, which is available at www.interscience.wiley.com.]

thermal performance of a heat exchanger. The work starts with the four configurations described earlier (CEP, PEC, CEC, PEP). Measuring both pressure drop and thermal flux transferred as a function of flow rates gives the global impact on performances.

Experimental set-up

As shown in Figure 7, the experimental setup constructed specially for this study is composed of a test section, hot and cold circuits, and the data acquisition system. Tap water was used as working fluid and balanced flow was taken for both hot and cold circuits. The flow rate ranged between 10×10^{-3} m^3 per min and 40×10^{-3} m^3 per min, corresponding to a channel Re from 800 to 3100 for the cold side. Two auxiliary heat exchangers (SWEP, 25 kW max) were installed for cooling the outlet cold water and for heating the outlet hot water to maintain the desired temperature difference. Water temperature in each tank was regulated by a three-way-valve (SAMSON SA, 3226 K) connected to and controlled by a PID controller (ASCON, M5 line). The connections of the piping system were designed such that parts can be easily modified and repaired. The tightness of the setup was verified before every test to avoid leakage. The test section is assembled to resist pressure and insulated by heat-

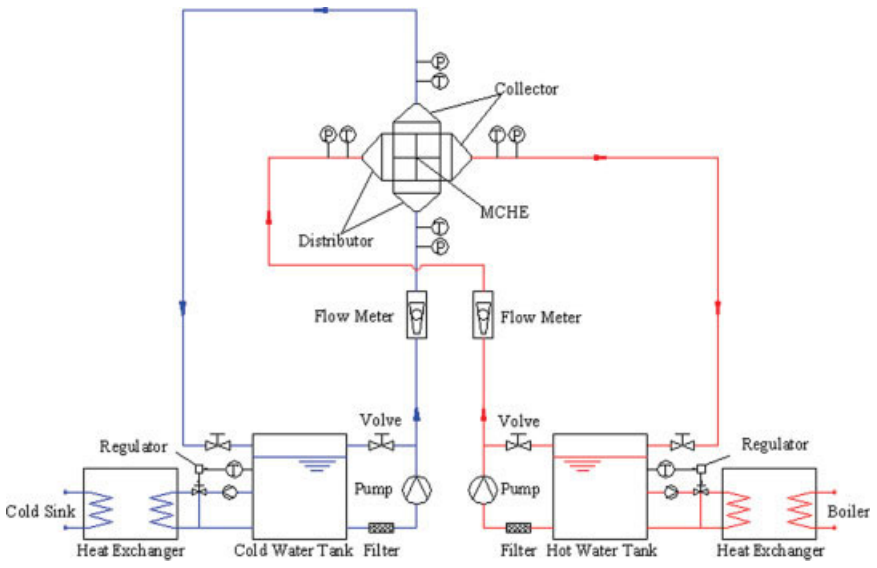

Figure 7. Sketch of the experimental setup.

[Color figure can be viewed in the online issue, which is available at www.interscience.wiley.com.]

Table 3. Range and Precision of Experimental Data

Parameter	Device	Range	Unit	Precision
Flow rate	KOBOLD DRG-1125 G4 L442 rotating vane flowmeter	$5–90 \times 10^{-3}$	$m^3\ min^{-1}$	±3% of full scale
Temperature	RTD-PT100 sensor 3 mm diameter × 100 mm long	−25–200	°C	0.5%
Pressure	KOBOLD SEN-3231 pressure sensor	0–10	Bar	±0.5% of full scale
Thermodynamic property	NBS/NRC steam tables (Haar et al.[33])	0–800	°C	
		0–10,000	Bar	

barrier materials to avoid heat loss to the environment. The calculated heat losses between the heat transferred by the hot side and received by the cold side were less than ±5%, implying that good heat balance was achieved.

Parameters measurement and uncertainties

The flow rate, temperature, and absolute pressure were measured. Flow rate was measured by calibrated rotating vane flow meters (KOBOLD DRG-1125 G4 L442) with plug-on display. The measure range is $5–90 \times 10^{-3}$ m^3 per min with the accuracy of ±3% of full scale. Pressure and temperature measuring points were located at the inlet and the outlet of the test section for the determination of the water state values. The temperatures were measured with RDT PT100 sensors, which were calibrated in melting ice at 0°C before the experiments and connected to a data-acquisition unit to record the mean temperatures of the fluids. Four pressure sensors (KOBOLD SEN-3231) with plug-on display were used to tract the isothermal absolute pressure. Once the temperature and the absolute pressure of the fluid are determined, other values of thermodynamic properties are calculated referring to NBS/NRC Steam Tables.[33] Details about the instruments and the uncertainties of the measurements are presented in Table 3.

The uncertainty analysis for the derived quantities was calculated following the Moffat method.[34] The uncertainty calculation showed that maximum of 4.1% for Reynolds number Re, 1% for the effectiveness (Eq. 7), and 0.5% for pressure drop Δp. It should be claimed here that these estimations are rather conservative because most uncertainties between channels generated by imperfections and irregularities in fabrication were considered to be at the minimum level.

Data reduction

The basic physical equations used to describe the heat transfer process of the exchanger are developed with the following simplifying assumptions:

- The fluid flow rate is steady.
- Heat transfer rate is steady.
- Heat loss between the system and environment is negligible.
- The kinetic energy and the potential energy changes of the fluids in and out of the heat exchanger are negligible.

The heat transferred from the hot side is given as the variation of the enthalpy of the fluid per unit time,

$$Q_{\text{hot}} = \dot{m}_{\text{hot}}(H_{\text{hot,in}} - H_{\text{hot,out}}) \tag{3}$$

and the heat received by the cold side is

$$Q_{\text{cold}} = \dot{m}_{\text{cold}}(H_{\text{cold,out}} - H_{\text{cold,in}}) \tag{4}$$

Here H is the specific enthalpy (J kg^{-1}) of the fluid. Since the heat balance was achieved, the average value between Q_{hot} and Q_{cold} was considered as the correct value.

$$Q_{\text{ave}} = \frac{Q_{\text{hot}} + Q_{\text{cold}}}{2} \tag{5}$$

The effectiveness of a heat exchanger is defined as the ratio of the actual heat transfer to the maximum possible heat transfer. For the balanced flow ($\dot{m}_{\text{hot}} = \dot{m}_{\text{cold}}$), Effectiveness can be rewritten as

$$\varepsilon = \frac{Q_{\text{ave}}}{Q_{\max}} = \frac{H_{\text{hot,in}} - H_{\text{hot,out}}}{H_{\text{hot,in}} - H_{\text{cold,in}}} = \frac{H_{\text{cold,out}} - H_{\text{cold,in}}}{H_{\text{hot,in}} - H_{\text{cold,in}}} \tag{6}$$

For crossflow heat exchangers with both fluids unmixed, the effectiveness can be expressed by the following relation (Kays and Crawford)[39]

$$\varepsilon = 1 - \exp\left[\frac{\exp(-\text{NTU}C^*\text{NTU}^{-0.22}) - 1}{C^*\text{NTU}^{-0.22}}\right] \tag{7}$$

where C^* is the ratio between maximum heat capacity $(\dot{m}Cp)_{\max}$ and minimum heat capacity of fluids $(\dot{m}Cp)_{\min}$. For balanced flow ($C^* = 1$), Eq. 7 becomes

$$\varepsilon = 1 - \exp\left[\frac{\exp(-\text{NTU}^{0.78}) - 1}{\text{NTU}^{-0.22}}\right] \tag{8}$$

The number of heat transfer units (NTU) can be expressed as

$$\text{NTU} = \frac{UA}{(\dot{m}Cp)_{\min}} \tag{9}$$

The actual heat transfer area and the overall heat transfer coefficient are denoted as A (5.68×10^{-2} m^2 in this case) and U, respectively. As a result, the overall heat transfer coefficient of the heat exchanger can be calculated by the following equation:

$$U = \frac{(\dot{m}Cp)_{\min}\,\text{NTU}}{A} \tag{10}$$

For proper heat exchanger design, heat transfer enhancement techniques improve the thermal performance, but generally they also increase the friction factor associated with the flow. As a result, heat transfer and pressure drop are two factors that should be considered together. Energy dissipated due to pressure drops is indicated by the *pump power per unit heat transfer surface area*,[35] which is defined as follows:

$$P = \frac{2\dot{m}\Delta p}{A} \tag{11}$$

Results and Discussion

Heat transfer

Figure 8 shows the overall heat transfer coefficients of the heat exchanger as a function of the average channel Re number of the cold side. Compared with the results of the thermal tests in pure laminar flow conditions,[22] similar tendency is observed. The overall heat transfer coefficients increase with the Re, mainly because of the reduced thermal boundary layer by the increasing flow velocity. Under the same Re conditions, the overall heat transfer coefficients of the configurations that involve constructal distributors/collectors (CEC, CEP, and PEC) are higher than that of the reference configuration PEP. The heat transfer intensification represented by the augmentation of the overall heat transfer coefficient is obvious. Configurations CEP and CEC have similar effect on the enhancement of heat transfer. Compared with the reference case, the overall heat transfer coefficient of these two configurations increases from about 29.0% to 21.2% when the Re increases from 800 to 3100. A noticeable feature is that among all the tested configurations, it is the PEC, integration of constructal collector at the outlet surface of the heat exchanger that has the best thermal performance. It can lead to an augmentation of about 45.2%–29.2% in overall heat transfer coefficient compared with the reference case.

The theoretical overall heat transfer coefficient is expressed by combined conduction and convection in the heat exchanger, by simply using the classic correlations and taking the entrance effect into consideration[36]:

$$\frac{1}{U} = \frac{1}{h_{\text{hot}}} + \frac{\delta}{k} + \frac{1}{h_{\text{cold}}} \tag{12}$$

$$h = 1.86\,\frac{\lambda}{d}\,(\text{Re}\,\text{Pr})^{1/3}\left(\frac{d}{l}\right)^{1/3}\left(\frac{\mu}{\mu_w}\right)^{0.14}\alpha \qquad (\text{Re} < 1600,\ \text{RePr}(d/l) > 10) \tag{13}$$

for laminar flow conditions and

$$h = 0.023\,\frac{\lambda}{d}\,\text{Re}^{0.8}\,\text{Pr}^{0.3}\,\alpha \quad (\text{Re} > 1600,\ 100 > \text{Pr} > 0.6) \tag{14}$$

for turbulent flow conditions. Here h is the convective heat transfer coefficient and α in Eqs. 13 and 14 is the correction factor for entrance effect:

$$\alpha = 1 + \left(\frac{d}{l}\right)^{0.7} \tag{15}$$

The term δ/k of Eq. 12 signifies the conduction resistance of the aluminium between two working fluids (negligible after calculation). The theoretical overall heat transfer coefficients are then calculated and plotted in the Figure 8. Note that the theoretical overall heat transfer coefficient corresponds generally to that of the reference configuration PEP.

This intensification can be contributed to three reasons. First, the classic correlations used concerns the single heat exchanger but not the distributor-exchanger-collector system. Actually, the integration of fluid distributor/collector adds more effective volume, which would augment the residence time of fluids in the heat exchanger system. Consequently, the heat transfer could be intensified by conduction. Second, the pressure drops generated in the distributor/collector lead to energy dissipation which is not negligible under high flow rate conditions. This frictional and singularity dissipation is transformed to the form of heat which adds extra transfer power to the heat exchanger system and augments the overall heat transfer coefficients. And above all, it may be attributed to the more uniform flow distribution because of the integration of constructal component. Flow maldistribution causes a loss of heat exchange effectiveness by not making use of the maximum temperature difference effectively. Ranganayakulu and Seetharamu[37,38] have given a detail analysis of the effects of flow maldistribution on thermal performance of a heat exchanger by the finite element method and also found that the performance deteriorations are quite significant.

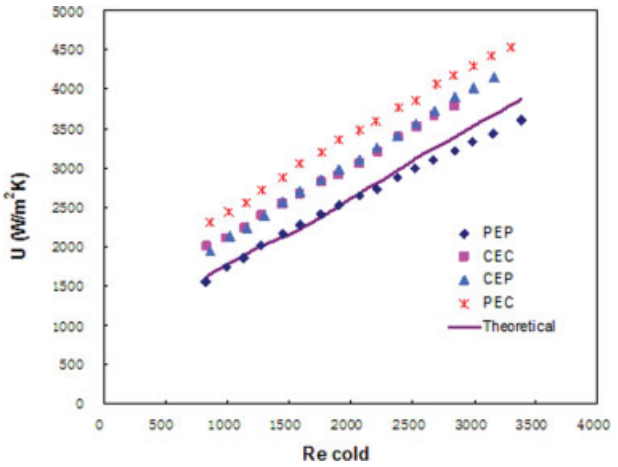

Figure 8. Overall heat transfer coefficient vs. channel Re number.

[Color figure can be viewed in the online issue, which is available at www.interscience.wiley.com.]

As have been demonstrated in the simulation section, the constructal component can achieve the most uniform flow distribution, whereas it functions as a fluid collector. In the CEC case that two constructal components are involved, the flow distribution in the channels of heat exchanger is determined by the inlet flow distributor. That is to say, the flow distribution quality of the CEC is similar to that of the CEP, less uniform than that of the PEC. This can explain why the CEC and the CEP has similar thermal performance but not as good as that of the PEC. By comparing the overall heat transfer coefficients of four tested configurations, the benefit of flow uniform distribution is obvious: the configuration PEC has the best thermal performance. This conclusion is not only valid under the pure laminar flow condition with small temperature difference as reported in Ref. 22, but also under a wide flow rate and Re range.

Pressure drop

Figure 9 shows the comparison of measured pressure drops for the test section. The pressure drop of each configuration increases with the increasing inlet flow rate. The integration of constructal component brings a considerable increase in

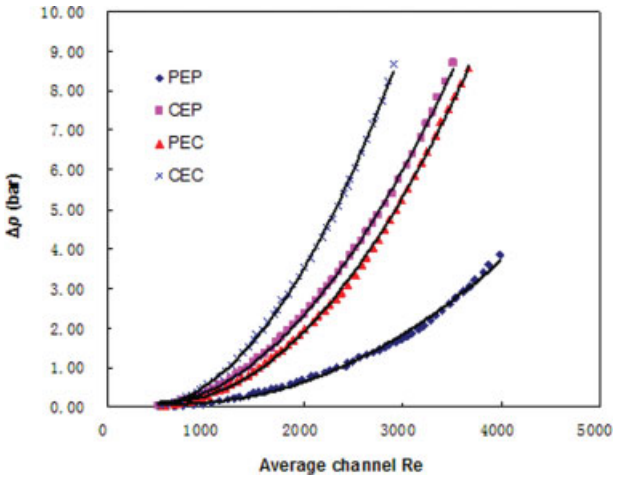

Figure 9. Pressure drops of various configurations vs. average channel Re number.

[Color figure can be viewed in the online issue, which is available at www.interscience.wiley.com.]

pressure drop, notably under high flow rate conditions. At the same inlet velocity, the configuration CEC involving two constructal components has consistently higher pressure drops than other configurations have. It reaches 8.68 bar at the average channel Re of 2900, 4.3 times higher than that of the reference PEP (1.64 bar); the pressure drops of the other two configurations PEC and CEP are 2.3 times (3.77 bar) and 2.0 times higher (3,28 bar) than that of the PEP, respectively. A comparison of the pressure drops between the test section with or without the heat exchanger inserted indicates that the frictional pressure drop in the channels of the heat exchanger is negligible compared with the total pressure drop. One can also easily tell the difference of the pressure drops in the constructal component and in the pyramidal distributor by comparing the pressure drops of the CEC and PEP. It is the complex multi-scale structure, and above all

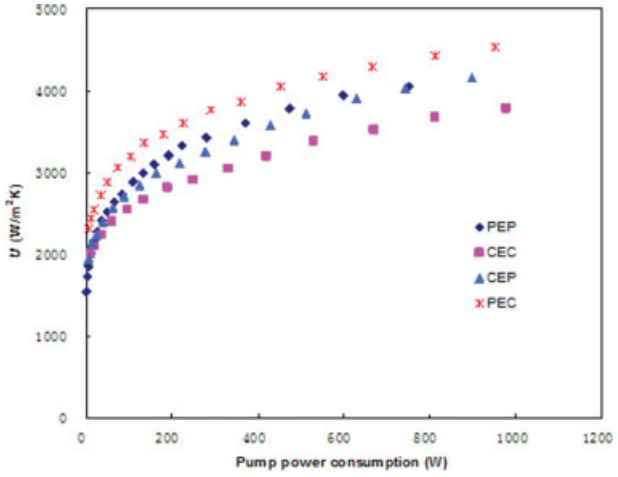

Figure 10. Overall heat transfer coefficient vs. pump power consumption.

[Color figure can be viewed in the online issue, which is available at www.interscience.wiley.com.]

the various singularities (bifurcations, elbows, downcomers) of the constructal component that causes the pressure drop increase under turbulent flow conditions.

Regression lines are fitted using second order polynomial type, as listed in Table 4 and plotted in Figure 9:

$$\Delta p = C_2\,\mathrm{Re}^2 + C_1\,\mathrm{Re} + C_0 \tag{16}$$

The square relativity (R^2) of each configuration is larger than 0.995, implying good agreement between the fitting curve and the experimental data.

From Figure 9, it can also be noted that, the pressure drop of the CEP is a little higher than that of the PEC under the same average channel Re condition. For example, at average channel Re of 3189, the pressure drop of the CEP reaches 6.83 bar, 0.64 bar higher than that of the PEC (6.19 bar). That is to say, the distributor case and the collector case do not generate the same pressure drops. Besides the difference caused by the temperature dependent viscosity, less vortex are produced and less energy is dissipated by the action of collection rather than that of distribution. This nonsymmetrical phenomenon is also observed and explained in our previous research.[21] However, the difference is not very significant compared with the total pressure drop under turbulent flow conditions.

Thermal-hydraulic balance

Heat transfer intensification by the integration of constructal components may be also at the cost of higher pump power dissipation. As a result, the thermal-hydraulic balance should be considered under operating condition in real-world engineering. Figure 10 shows the overall heat transfer coefficients of various configurations as a function of pump power consumption. The overall heat transfer coefficients increase pump power consumption increases. At this point, for certain heat transfer surface area, heat transfer could be enhanced by consuming more pump power to increase the velocity of the working fluid in the channels, just as most of active heat transfer enhancement techniques do.

In addition, it also discloses that the energy dissipated (pressure drop) in the constructal component increases rapidly with the increasing flow rate. It would cause an energy loss rather than gain even though it still intensifies the heat transfer. The constructal distributor/collector is not "*almighty*." To use it or not depends on certain working conditions of the heat exchanger system. In our cases investigated, the integration of construtal components is preferable for pump power dissipation less than 200 W, corresponding to a value of average channel Re less than about 2000 (laminar flow condition).

Table 4. Correlations for Pressure Drops of Various Configurations

Configuration	Correlation	R^2
CEP	$\Delta p = 9 \times 10^{-7}\,\mathrm{Re}^2 - 0.0006\mathrm{Re} + 0.1253$	0.9997
PEC	$\Delta p = 9 \times 10^{-7}\,\mathrm{Re}^2 - 0.001\mathrm{Re} + 0.4002$	0.9994
CEC	$\Delta p = 1 \times 10^{-6}\,\mathrm{Re}^2 - 0.001\mathrm{Re} + 0.2138$	0.9995
PEP	$\Delta p = 3 \times 10^{-7}\,\mathrm{Re}^2 - 0.0005\mathrm{Re} + 0.2413$	0.9953

Meanwhile, to achieve a certain value of the overall heat transfer coefficient, PEC consistently consumes less pump power compared with other configurations. Better thermal performance could be achieved at the cost of relatively low pump power consumption by the integration of constructal collector at the outlet surface of the heat exchanger. In fact, the configuration PEC can equalize the flow distribution among the channels of the exchanger, leading to the relatively better thermal performance. Based on the balanced consideration of heat transfer intensification and pump power consumption, the configuration PEC is relatively the most advantageous.

Conclusion

Flow maldistribution, heat transfer intensification, and hydraulic performance of the mini heat exchanger with constructal component integrated are numerically and experimentally investigated. Based on the discussions mentioned earlier, following conclusions could be reached.

The numerical comparative study on the flow distribution behavior shows that the flow direction in the constructal component has a great influence on the final distribution quality. The constructal component functioning as fluid collector can approach more uniform and stable flow distribution. Experimental visualization test also confirms that flow maldistribution exists in the distributor case and share the same manner as the CFD simulation results.

This more uniform and stable flow distribution guaranteed by the integration of constructal collector can enhance the overall heat transfer coefficient of the heat exchanger from 45.2% to 29.2% under various Re conditions. The heat transfer intensification by flow uniform distribution is significant.

Inner structure complexity of the constructal component causes considerable pressure drops and the extra pump power consumption of the system with the increasing of the total flow rate. The results show that the integration of constructal component may have its scope of application and may be more interesting in low Re number range (laminar flow). Based on a balanced consideration of heat transfer intensification and pump power consumption, the integration of constructal collector at the outlet of the heat exchanger is relatively the most advantageous both under laminar and turbulent flow conditions.

Acknowledgments

This work is supported by the French ANR (Agence National de la Recherche) within the "programme non thématique 2005, Projet n°NT05-3_41570) and Allocation de Recherche 2005 Cluster ENERGIE, Région Rhône-Alpes, France.

Notation

A = heat transfer surface, m^2
C^* = ratio between maximum heat capacity and minimum heat capacity of fluids
D_i = relative flow rate deviation at outlet port i, dimensionless
D_g = flow maldistribution factor, dimensionless
d = diameter of channel, m
f = flow rate $m^3\ s^{-1}$
H = specific enthalpy, J kg^{-1}
h = convective heat transfer coefficient W $m^{-2}\ K^{-1}$
l = length of the heat exchanger channel, m
$\dot{m}$ = mass flow rate of working fluid, kg s^{-1}
NTU = number of heat transfer unit
P = pump power consumption per unit transfer area, W m^{-2}
Q = heat transfer, W
Re = Reynolds number based on channel diameter of the exchanger
T = temperature, °C
U = overall heat transfer coefficient, W $m^{-2}\ K^{-1}$

Greek letters

a = entrance effect factor, dimensionless
β = surface area density, $m^2\ m^{-3}$
ε = effectiveness, dimensionless
δ = thickness, m
μ = viscosity, kg $m^{-1}\ s^{-1}$
μ_w = viscosity in wall temperature, kg $m^{-1}\ s^{-1}$
Δp = pressure drop, bar

Subscripts

ave = average
gen = generation
in = inlet
out = outlet
cold = cold fluid
hot = hot fluid
max = maximum
min = minimum
i = port index

Literature Cited

1. Fleming RB. The effect of flow distribution in parallel channels of counter-flow heat exchangers. *Adv Cryog Eng*. 1967;12:352.
2. Chiou JP. Thermal performance deterioration in crossflow heat exchanger due to flow nonuniformity. *ASME J Heat Transfer*. 1978;100:580–587.
3. Chiou JP. The advancement of compact heat exchanger theory considering the effects of longitudinal heat conduction and flow nonuniformity effects. In: Shah RK, McDonald CF, Howards CP, editors. *Compact Heat Exchangers-Mechanical Engineering-History, Technological Advancement and Mechanical Design Problems*. New York: ASME, 1980:101–121.
4. Mueller AC, Chiou JP. Review of various types of flow maldistribution in heat exchangers. *Heat Transfer Eng*. 1988;9:36–50.
5. Thonon B, Mercier P. Plate heat exchangers: 10 years of research at GRETh, Part 2: Sizing and flow maldistribution. *Revue Générale de Thermique*. 1996;35:561–568.
6. Lalot S, Florent P, Lang SK, Bergles AE. Flow maldistribution in heat exchangers. *Appl Therm Eng*. 1999;19:847–863.
7. Bobbili PR, Kumar PK, Das SK. Effect of flow distribution to the channels on the thermal performance of a plate heat exchanger. *Chem Eng Process*. 2002;41:49–58.
8. Bobbili PR, Sunden B, Das SK. An experimental investigation of the port flow maldistribution in small and large plate package heat exchangers. *Appl Therm Eng*. 2006;26:1919–1926.
9. Jiao A, Zhang R, Jeong SK. Experimental investigation of header configuration on flow maldistribution in plate-fin heat exchanger. *Appl Therm Eng*. 2003;23:1235–1246.
10. Kulkarni T, Bullard C, Cho K. Header design tradeoffs in microchannel evaporators. *Appl Therm Eng*. 2004;24:759–776.
11. Wen J, Li Y. Study of flow distribution and its improvement on the header of plate-fin heat exchanger. *Cryogenics*. 2004;44:823–831.
12. Jiao A, Baek S. Effects of distributor configuration on flow maldistribution in plate-fin heat exchangers. *Heat Transfer Eng*. 2005;26:19–25.
13. Srihari N, Bobbili PR, Sunden B, Das SK. Transient response of plate heat exchangers considering effect of flow maldistribution. *Int J Heat Mass Transfer*. 2005;48:3231–3243.

14. Jung J, Jeong S. Effect of flow mal-distribution on effective NTU in multi-channel counter-flow heat exchanger of single body. *Cryogenics*. 2007;47:232–242.
15. Zhang Z, Li Y. CFD simulation on inlet configuration of plate-fin heat exchangers. *Cryogenics*. 2003;43:673–678.
16. Wen J, Li Y, Wang S, Zhou A. Experimental investigation of header configuration improvement in plate-fin heat exchanger. *Appl Therm Eng*. 2007;27:1761–1770.
17. Tereda FA, Das SK, Sunden B. Experimental study on port to channel flow distribution of plate heat exchanger. In: Shah SK, Ishizuka M, Rudy TM, Wadekar VV, editors. *Proceedings of Fifth International Conference on Enhanced, Compact and Ultra-Compact Heat Exchangers: Science*, Engineering and Technology, Hoboken, NJ, 2005:208–214. September 11–16, 2005 – Whister, BC Canada.
18. Galeazzo F, Miura RY, Gut J, Tadini CC. Experimental and numerical heat transfer in a plate heat exchanger. *Chem Eng Sci*. 2006;61: 7133–7138.
19. Wang S, Wang S. Distribution optimization for plate-fin catalytic combustion heat exchanger. *Chem Eng J*. 2007;131:171–179.
20. Jones B, Lee P, Garimella S. Infrared micro-particle image velocimetry measurements and predictions of flow distribution in a microchannel heat sink. *Int J Heat Mass Transfer*. 2008;2–8:1877–1887.
21. Luo L, Fan Y, Zhang W, Yuan X, Midoux N. Integration of constructal distributors to a mini crossflow heat exchanger and their assembly configuration optimization. *Chem Eng Sci*. 2007;62:3605–3619.
22. Luo L, Fan Z, Le Gall H, Zhou X, Yuan W. Experimental study of constructal distributor for flow equidistribution in a mini crossflow heat exchanger (MCHE). *Chem Eng Process*. 2008;47:229–236.
23. Habib MA, Ben-Mansour R, Said SAM, Al-Bagawi JJ, Al-Mansour KM. Correlations of flow distribution parameters in an air cooled heat exchanger. *Int J Numer Methods Fluids*. 2008;56:143–165.
24. Kim MS, Lee KS, Song S. Effect of pass arrangement and optimization of design parameters on the thermal performance of a multipass heat exchanger. *Int J Heat Fluid Flow*. 2008;29:352–363.
25. Tondeur D, Luo L. Design and scaling laws of ramified fluid distributors by the constructal approach. *Chem Eng Sci*. 2004;59:1799–1813.
26. Luo L, Tondeur D. Optimal distribution of viscous dissipation in a multi-scale branched fluid distributor. *Int J Thermal Sci*. 2005; 44:1131–1141.
27. Bejan A. Constructal theory network of conducting paths for cooling a heat generating volume. *Int J Heat Mass Transfer*. 1997;40:799–816.
28. Bejan A. *Shape and Structure, from Engineering to Nature*. UK: Cambridge University Press, 2000.
29. Bejan A, Lorente S. Constructal theory of generation of configuration in nature and engineering. *J Appl Phys*. 2006;100:041301.
30. André JC, Corbel S. (Collective). *Stéréophotolithographie Laser*. Paris: Polytechnica, 1994.
31. Dufaud O, Corbel S. Dispositif de déposition de couches de suspensions de céramiques appliqué a la stéréolithographie. *Can J Chem Eng*. 2004;82:986–993.
32. Luo L, Tondeur D, Le Gall H, Corbel S. Constructal approach and multi-scale components. *Appl Therm Eng*. 2006;27:1708–1714.
33. Haar L, Gallagher JS, Kell GS. *NBS/NRC Steam Tables: Thermodynamic and Transport Properties and Computer Programs for Vapor and Liquid States of Water in SI Units*. Washington: Hemisphere Publishing Corporation, 1984.
34. Moffat RJ. Describing the uncertainties in experimental results. *Exp Therm Fluid Sci*. 1988;1:3–17.
35. Wang J, Hirs GG, Rollmann P. The performance of a new gas to gas heat exchanger with strip fin. *Energy Convers Manage*. 1999;40:1743–1751.
36. Holman JP. *Heat Transfer*, 9th ed. New York: McGraw-Hill, 2002.
37. Ranganayakulu CH, Seetharamu KN. The combined effects of longitudinal heat conduction, flow nonuniformity and temperature nonuniformity in crossflow plate-fin heat exchangers. *Int Commun Heat Mass Transfer*. 1999;26:669–678.
38. Ranganayakulu CH, Seetharamu KN. The combined effects of wall longitudinal heat conduction, inlet fluid flow nonuniformity and temperature nonuniformity in compact tube-fin heat exchangers: a finite element method. *Int J Heat Mass Transfer*. 1999;42:263–273.
39. Kays WM, Crawford ME, Connective Heat and Mass Transfer. 3rd ed. McGraw-Hill, 1993. ISBN: 0070337217.

Manuscript received Feb. 4, 2008, and revision received May 21, 2008.